AGU
ADVANCING EARTH AND SPACE SCIENCE

Geophysical Research Letters®

Key Points:
- Equilibration has a neutral or depleting effect in the first stages of the downdraft, and an enriching effect later
- The overall contribution of equilibration is smaller than that of evaporation
- Equilibration might play a greater role when the concentration of cloud condensation nuclei is lower

Correspondence to:

G. Torri,
gtorri@hawaii.edu

Isotopic Equilibration in Convective Downdrafts

Giuseppe Torri[1] (ORCID)

[1]Department of Atmospheric Sciences, University of Hawai'i at Mānoa, Honolulu, HI, USA

Abstract While it is becoming increasingly clear that stable water isotopologues are important tools in the study of atmospheric convection, many questions remain on how different processes affect them. This work is focused on water vapor isotopes in precipitation-driven downdrafts. Using idealized simulations, the contributions of rain evaporation and liquid-vapor equilibration processes are analyzed. It is shown that rain evaporation tends to deplete water vapor isotopes throughout the downdraft's descent, whereas equilibration has a neutral or depleting effect in the first half of the downdraft's life cycle and an enriching one in the second half. The total contribution of the two processes is then discussed, and it is argued that equilibration has an overall small effect compared to rain evaporation. Finally, using two sensitivity experiments, it is shown that the role played by equilibration varies significantly in regimes with different concentrations of cloud condensation nuclei.

Plain Language Summary Water naturally exists in various forms which differ only by their mass. These small discrepancies provide water molecules with slightly different physical properties. This fact might be used to gain important information about the history of water vapor molecules in an air parcel. This study focuses on descending air currents that occur in storms and aims at clarifying how two microscopic processes might affect water molecules of various masses differently. The first process is the evaporation of rain, which takes place below clouds when water molecules flow from the liquid to the vapor phase. The other process, known as equilibration, is an exchange of heavier water molecules between the liquid and the vapor that takes place below clouds even without rain evaporation. The results discussed here could help interpret computer model simulations and observational data of convective storms.

1. Introduction

The importance of cumulus clouds in the climate system can hardly be overemphasized. From the interaction with large-scale circulations, or its effect on the planetary radiation budget, to its impact on the hydrometeorology of a given region, cumulus convection is one of the key players in the Earth's climate (e.g., Arakawa, 2004; Frank, 1983; Garstang & Betts, 1974; Siebesma et al., 2020). A deeper understanding of cumulus clouds is thus needed to better understand the global climate and to forecast its future evolution. In spite of the progress made in recent decades (Siebesma et al., 2020), however, there remain questions to be fully clarified.

Cumulus clouds owe part of their complexity to their structure, being formed by different phases of water which interact with each other and with the environment on multiple, non-separable scales (Siebesma et al., 2020). Rain evaporation is a particularly important example: in sub-saturated conditions, the exchange of water molecules between raindrops and the surrounding vapor can lead to a significant decrease of the rainfall reaching the surface and to the formation of convective downdrafts (Betts & Silva Dias, 1979; Knupp, 1988; Torri & Kuang, 2016a). When they reach the surface, downdrafts give rise to cold pools, key ingredients in the formation of new convective cells (Jeevanjee & Romps, 2015; Schlemmer & Hohenegger, 2014; Tompkins, 2001; Torri et al., 2015). Large rain evaporation rates can also produce particularly strong downdrafts, which become a threat to the people on the ground (Fujita, 1985, 1986; Wakimoto et al., 1994). In spite of their importance, these exchanges are challenging to measure and typically happen on scales that are too small to be fully resolved by climate models (Siebesma et al., 2020).

In the study of microphysical processes in cumulus clouds, water isotopologues can be powerful tools (e.g., Galewsky et al., 2016, and references therein). Slight differences in their masses provide isotopologues with different chemical and physical properties. Certain processes can thus differentiate between water isotopologues, a phenomenon known as *isotope fractionation* (Hoefs, 2015). It is customary to distinguish between two types of fractionation. Isotope exchanges between different species or compounds in chemical equilibrium constitute

what is called *equilibrium fractionation*. Those exchanges that happen out of equilibrium, and which are often unidirectional, are known as *kinetic fractionation* processes.

As rain falls in sub-saturated conditions, two types of microphysical processes happen that can affect its isotopic composition. The first is due to kinetic fractionation caused by rain evaporation: lighter water isotopologues have a higher vapor pressure and greater diffusivities, and thus evaporate preferentially compared to heavier isotopologues (Hoefs, 2015). The second is driven by the tendency of the liquid-vapor system to reach equilibrium and is usually referred to as *equilibration* (Hoefs, 2015). A clear understanding of how these two processes affect the isotopic composition of rain and of the water vapor in the surrounding downdrafts is needed in order to use water isotopologues to study and estimate rain evaporation.

The study of evaporation and equilibration processes and their effects on the isotopic composition of rain and water vapor has been undertaken by different authors using measurements taken in a laboratory (Friedman et al., 1962; Stewart, 1975), observations of rainfall (Salamalikis et al., 2016; Wang et al., 2016; Zhu et al., 2021) and water vapor (Aemisegger et al., 2015; Graf et al., 2019; Tremoy et al., 2014). Although substantial progress has been made, data interpretation is often limited by the use of relatively simple conceptual frameworks. For example, in some models, convection is parameterized or rain is assumed in isotopic equilibrium with its surrounding vapor (e.g., Bolin, 1959; Bolot et al., 2013; Lee & Fung, 2008; Salamalikis et al., 2016).

In recent years, more sophisticated numerical models have been developed that simulate atmospheric water isotopologues at a global scale (Nusbaumer et al., 2017; Pfahl et al., 2012), as well as at a more local scale, potentially with a small enough grid spacing to explicitly resolve convection (Blossey et al., 2010; Moore et al., 2016). While microphysical processes remain parameterized in these higher-resolution models, explicitly resolving convection provides a more complete picture of the behavior of water isotopologues in convective clouds and related phenomena (Risi et al., 2020, 2021; Torri, 2021). In turn, this could provide a more refined theoretical lens to interpret data.

Torri (2021) examined the impact of microphysical processes and mixing on the isotopic composition of downdraft water vapor and found that they were of similar magnitudes. While mixing was shown to have an overall enriching effect, microphysics had a depleting effect in the first part of the downdraft and enriching in the second part. However, the diagnostic tools used by Torri (2021) did not clarify how individual microphysical processes, such as rain evaporation and equilibration, contributed, which left some doubts on how to interpret water vapor isotopic compositions.

This study investigates this specific problem, which will be articulated in two questions:

- What are the relative roles of evaporation and equilibration in modulating water vapor isotopes in convective downdrafts?
- How are those roles sensitive to microphysical parameters, such as the concentration of cloud condensation nuclei?

These questions will be addressed through a series of numerical experiments conducted with an isotope-enabled cloud-resolving model (CRM) and a Lagrangian particle model.

2. Methods

2.1. The Eulerian Model: SAMiso

The simulations discussed in this study are conducted with the System for Atmospheric Modeling (SAM), version 6.10.9 (Khairoutdinov & Randall, 2003). The model solves the anelastic equations of motion, and its prognostic variables are liquid water static energy, non-precipitating, and precipitating total water. Periodic boundary conditions are imposed in the horizontal directions and with a rigid lid at the model top, with a sponge layer placed in the upper third of the domain. Advection is represented by a fifth-order scheme (Yamaguchi et al., 2011), and subgrid-scale effects are parameterized using a prognostic turbulent kinetic energy 1.5-order closure scheme. Surface sensible and latent heat fluxes are computed using the Monin-Obukhov formula assuming a fixed oceanic surface with sea surface temperature (SST) of 301.15 K. Radiative processes are parameterized using the Rapid Radiative Transfer Model for Global climate model applications (RRTM) scheme (Iacono et al., 2008; Mlawer et al., 1997).

Microphysical processes are represented using the Thompson scheme (Thompson et al., 2008), which predicts the mixing ratios of water vapor, cloud liquid water, cloud ice, rain, snow, and graupel, as well as the number concentrations of rain and cloud ice. The particular scheme used in this study was modified to also include water isotopologues (Blossey et al., 2010; Moore et al., 2016). Fractionation is included for condensation and deposition onto ice and for evaporation of rain and cloud water. Riming, freezing, melting, and sublimation of frozen hydrometeors are assumed to be non-fractionating (Blossey et al., 2010; Bony et al., 2008; Pfahl et al., 2012). Furthermore, cloud liquid water and water vapor are kept in equilibrium at all time steps (Blossey et al., 2010). This isotope-enabled version of SAM will be referred to as SAMiso.

2.2. The Lagrangian Model: LPDM

SAMiso is coupled to the Lagrangian Particle Dispersion Model (LPDM) (Nie & Kuang, 2012; Torri et al., 2015; Torri & Kuang, 2016b). The Lagrangian particles are considered as a passive element in the simulation and do not feed back on the dynamics or the thermodynamics of SAMiso.

At the beginning of each simulation, particles are randomly distributed in the vertical pressure coordinate, which makes it possible to think of each as being embedded in a parcel of air of a given mass (Torri & Kuang, 2016b). In addition, particles are assigned a temperature and a mixing ratio for each water vapor isotopologue equal to the value of the grid box in which the particle is contained.

The particle positions and thermodynamic properties are then updated at each time step using the three-dimensional velocity fields and thermodynamic tendencies computed by SAMiso. By updating the thermodynamic variables for each particle following these methods, it has been shown that the average values of those variables computed over all the particles in any model grid box match the values of the Eulerian fields produced by SAMiso in the same box (Torri & Kuang, 2016b).

2.3. The Simulations

The simulations used in this work are of two kind: a set of 5 control simulations that will be referred to as the *control ensemble*, and two sensitivity experiments to test how the main conclusions are sensitive to raindrop sizes. This will be achieved by varying the concentration of cloud condensation nuclei (CCN).

Similarly to Torri (2021), all the simulations are run in a $96 \times 96 \times 30$ km^3 domain. The horizontal resolution is 250 m, whereas the vertical resolution varies from 31 to 500 m, the latter being reached at approximately 10 km of altitude. The time resolution is 3 s. The diurnal cycle of insolation is removed by fixing the zenith angle at 51.7° and by decreasing the solar constant to 685 W m^{-2} (Tompkins & Craig, 1998). Mean winds are initialized at zero, and no nudging or large-scale forcing is imposed. The LPDM is initialized with 512 particles in each column. For the control ensemble, each simulation is run with a CCN concentration $N_c = 100$ cm^{-3}, whereas for the two sensitivity experiments CCN concentrations are $N_c = 10$ cm^{-3} (NC10) and $N_c = 1,000$ cm^{-3} (NC1000).

Each simulation is first run for 50 days, until radiative-convective equilibrium (RCE) is reached. To reduce storage requirement, SAMiso is run without the LPDM during this step. Different ensemble members are obtained by adding random perturbations of liquid water static energy and water vapor mixing ratio at the beginning of each simulation. SAMiso is then restarted with the LPDM and run for 12 hr. Three-dimensional Eulerian and Lagrangian output data are saved every minute of model time.

2.4. Selecting Downdraft Particles

In this work, only those downdrafts that contribute to the formation of cold pools in the boundary layer are considered. This is achieved by first identifying *cold pool cores*, defined as grid boxes where the density potential temperature anomaly with respect to the horizontal mean, θ'_ρ, is lower than -1 K, and the precipitating water mixing ratio, r_p, is greater than 0.3 g kg^{-1} (Torri, 2021). The *subcloud layer* is defined as the bottom portion of the model domain where the temporal and horizontal averaged mass mixing ratio of non-precipitating hydrometeors (e.g., cloud droplets), r_n, is smaller than 10^{-3} g kg^{-1}.

Whenever a particle is found in a cold pool core, it is flagged, and its previous history is examined until the particle first acquired negative vertical velocity. The height at which this happens, called *initial height* (Torri, 2021;

Torri & Kuang, 2016a), is used to group particles in this work. Given the turbulent nature of downdrafts, a tolerance of 1 min is used to decide when the initial descent of a particle starts: if the condition of negative vertical velocity is violated for more than that, the tracking stops; otherwise, it continues. Sensitivity tests were conducted using time windows of 3 and 5 min, but no qualitative differences were noted (not shown).

2.5. Diagnosing Equilibration and Evaporation Contributions

Following Torri (2021), the roles of equilibration and evaporation for downdraft vapor are assessed by diagnosing their contributions to the Lagrangian derivative of $\ln(R_x)$:

$$\frac{D\ln(R_x)}{Dt} = \sum_i \left(\frac{S_{x,i}}{r_x} - \frac{S_{v,i}}{r_v} \right), \tag{1}$$

where i indicates either diffusion, mixing, evaporation, or equilibration, r_x (r_v) the mixing ratio of a heavier (lightest) water isotopologue, and $S_{x,i}$ ($S_{v,i}$) represent the tendency due to one of the four above-listed processes. Given the focus of this work, only the tendencies due to evaporation and equilibration will be considered.

Diffusive exchanges of the lighter isotope between liquid and vapor in a grid box can be described as:

$$\frac{dr_l}{dt} = C_l f D_v \left(\frac{1 - \beta_l}{1 + b_l} \right) (S_l - 1) = -S_{v,ev}, \tag{2}$$

where r_l is the liquid water mixing ratio, f is a ventilation factor, D_v the molecular diffusivity, C_l is a factor proportional to the main raindrop radius, and S_l is the ratio between vapor density and the saturation vapor density at infinity, which is roughly equal to relative humidity. For more details on how Equation 2 is derived, the reader is referred to Gedzelman and Arnold (1994) and Blossey et al. (2010), although slight variations of this formulation are likely ubiquitous in the literature. The factors b_l and β_l are related to changes in temperature caused by evaporation, and, since their detailed formulation is not relevant here, the reader is referred to Blossey et al. (2010) for a more in-depth discussion.

The equation regulating the liquid-vapor exchanges for heavier isotopes involves equilibration processes as well (cf. Equation B19 in Blossey et al. (2010)):

$$\frac{dr_{l,x}}{dt} = C_l f_x D_{x,v} \left[\frac{r_{v,x}}{r_v} S_l - \frac{r_{l,x}}{r_l} \frac{1}{\alpha_l} \left(1 + (b_l + \beta_l) \frac{S_l - 1}{1 + b_l} \right) \right], \tag{3}$$

where $r_{l,x}$ is the liquid water mixing ratio for heavier isotopes, f_x and $D_{x,v}$ are, respectively the ventilation factor and the molecular diffusivity for the heavier isotope, and α_l is the equilibrium fractionation factor over liquid water.

By adding and subtracting $S_l R_l / \alpha_l$ in the bracketed term of Equation 3, and through some algebraic manipulations, the equation can be re-written as:

$$\frac{dr_{l,x}}{dt} = C_l f_x D_{x,v} \frac{R_l}{\alpha_l} \left[\left(\frac{\alpha_l R_v}{R_l} - 1 \right) S_l + \left(\frac{1 - \beta_l}{1 + b_l} \right) (S_l - 1) \right] = -(S_{x,eq} + S_{x,ev}). \tag{4}$$

Thanks to these re-arrangements, the changes to $r_{l,x}$, and, consequently, to $r_{v,x}$ can be written as the sum of two terms, $S_{x,eq}$ and $S_{x,ev}$. Considering that the former is zero when the liquid is in equilibrium with the surrounding vapor, and that the latter is zero when the vapor is saturated, these will be interpreted as the contribution due to equilibration and to evaporation in Equation 1.

The overall role of equilibration and evaporation in a downdraft will be assessed by computing the differences between the final and the initial isotopic composition of downdraft particles. Assuming that the isotopic ratio of a particle at its entrance in the downdraft is $R_{x,0} = r_{x,0}/r_{v,0}$, its final isotopic ratio can be written as:

$$R_{x,f} = \frac{r_{x,f}}{r_{v,f}} = \frac{r_{x,0} + \sum_i \Delta r_{x,i}}{r_{v,0} + \sum_i \Delta r_{v,i}}, \tag{5}$$

where i refers to either diffusion, mixing, evaporation or equilibration, and $\Delta r_{x,i}$ and $\Delta r_{v,i}$ are overall changes to the mixing ratios of a heavy water isotopologue and of the lightest water isotopologue that occur throughout the downdraft's descent. By taking the difference between the final and the initial isotope ratio, one obtains:

$$\Delta R = R_{x,f} - R_{x,0} = \frac{\sum_i (\Delta r_{x,i} - R_{x,0}\Delta r_{v,i})}{r_{v,f}}. \tag{6}$$

Each term in the sum on the right hand side of Equation 6 will be considered as an estimate of the changes in the downdraft isotopic composition due to a particular process.

2.6. The $\Delta\delta$ Δd-Diagram

A recent study by Graf et al. (2019) has suggested a new method to assess the importance of equilibration effects on the isotopic composition of water vapor and rainfall. One of the tools used by the authors was called the $\Delta\delta\Delta d$-diagram, where the abscissa of each point represents the difference between the isotopic composition of the equilibrium vapor from precipitation near the surface and the composition of the vapor near the surface, $\Delta\delta = \delta^2H_{p,eq} - \delta^2H_{v,sfc}$, and the ordinate represents a similar difference but for deuterium excess instead, $\Delta d = d_{p,eq} - d_{v,sfc}$.

In their work, Graf et al. (2019) show that, for data points that have simultaneously $\Delta d \leq 0$ and $\Delta\delta \geq 0$, thus in the fourth quadrant of the $\Delta\delta\Delta d$-diagram, evaporation played a dominant role. On the other hand, those points for which $\Delta d \sim 0$ and $\Delta\delta \sim 0$ were closer to isotopic equilibrium. This method will be used as a consistency check on the conclusions reached using the Lagrangian diagnostics described above.

3. Results

The four panels in Figure 1 represent the contributions of equilibration and evaporation to the isotopic composition of downdraft particles as defined in Equation 1. Figures 1a and 1b refer to the contributions to $\ln R_{2H}$, whereas Figures 1c and 1d to those to $\ln R_{18O}$; Figures 1a and 1c represent the contributions due to equilibration, whereas Figures 1b and 1d those due to evaporation.

In order to construct these figures, downdraft particles are first grouped by their initial height. Then, for each initial height, the contributions at every height are averaged over all the particles across the control ensemble. The results are shown as a function of initial height (x-axis) and altitude during the downdraft descent (y-axis). To avoid confounding effects due to averaging over small samples, points for which the density of particles is lower than 10^{-1} m^{-2} are ignored.

Figures 1b and 1d show that rain evaporation tends to have a consistently depleting effect for both water vapor isotopes in convective downdrafts. The contributions are particularly large for particles descending from heights greater than 2 km.

Figure 1a suggests that for ^{2}H isotopes, the equilibration term is roughly of the same magnitude as evaporation, but its sign changes during the descent of the downdraft: equilibration depletes downdrafts in the early part of the descent, and enriches them in the second part. This is particularly true for particles with an initial height greater than approximately 1.5 km. For particles descending from a smaller height, the positive contributions seem to dominate. In the case of ^{18}O isotopes, equilibration appears to have an overall enriching effect, albeit of a smaller magnitude than evaporation.

Figure 2a shows the cumulative distribution function of the age of cold pool cores (x-axis) when particles of different initial heights (y-axis) enter them. The age of a cold pool core is determined by counting the time steps elapsed since the particular core was first detected. The black line in the figure represents the median cold pool core age encountered by particles with different initial heights. For particles with an initial height lower than 1 km, the median age is less than 40 min. For particles descending from greater altitudes, the median cold pool core age is between approximately 40 and 60 min.

The overall role played by evaporation and equilibration on downdraft water vapor isotopes, as described in Equation 6, is shown as a function of particles' initial heights (y-axis) in Figure 2b. The lines in the figure show
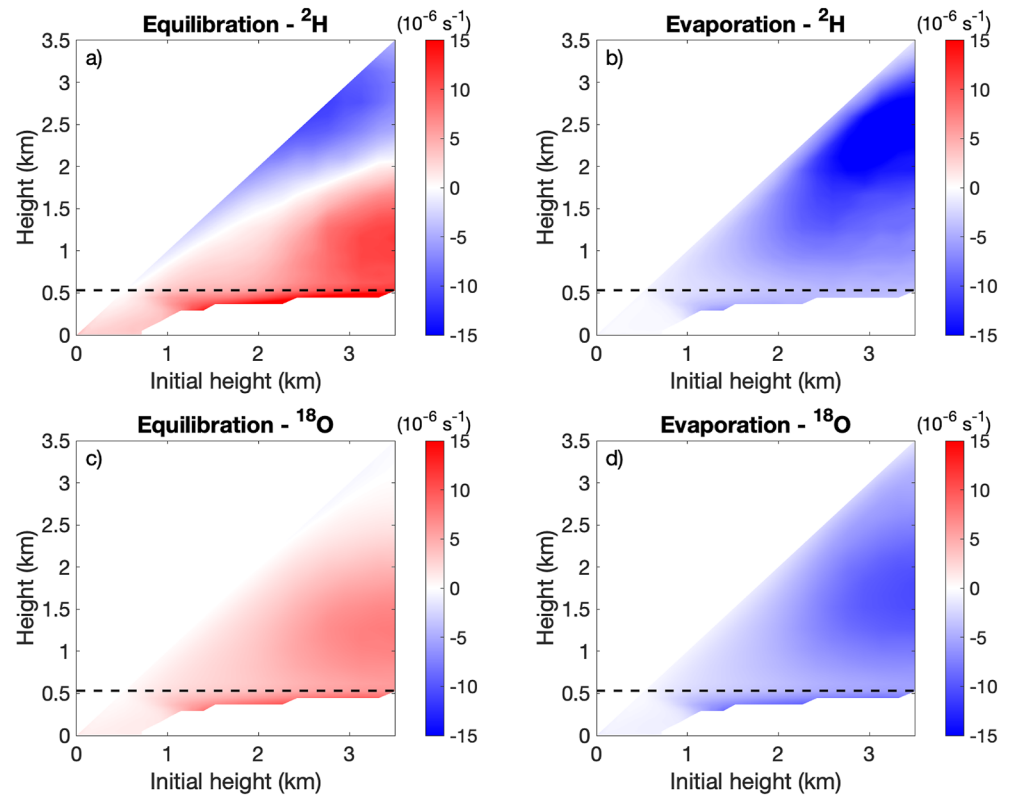
Figure 1. (a and c) Contributions of equilibration and (b and d) evaporation of rain to the evolution of $\ln R$ in convective downdrafts. The top row (a and b) refers to the ^{2}H isotope, whereas the bottom row (c and d) to the ^{18}O isotope. The horizontal dashed line represents the height of the subcloud layer top.

the total change in isotope ratio due to evaporation (continuous lines) and equilibration (dashed lines) for particles descending from different heights and for ^{2}H (blue) as well as ^{18}O isotopes (red). The figure suggests that, on the whole, rain evaporation plays a dominant role compared to equilibration.
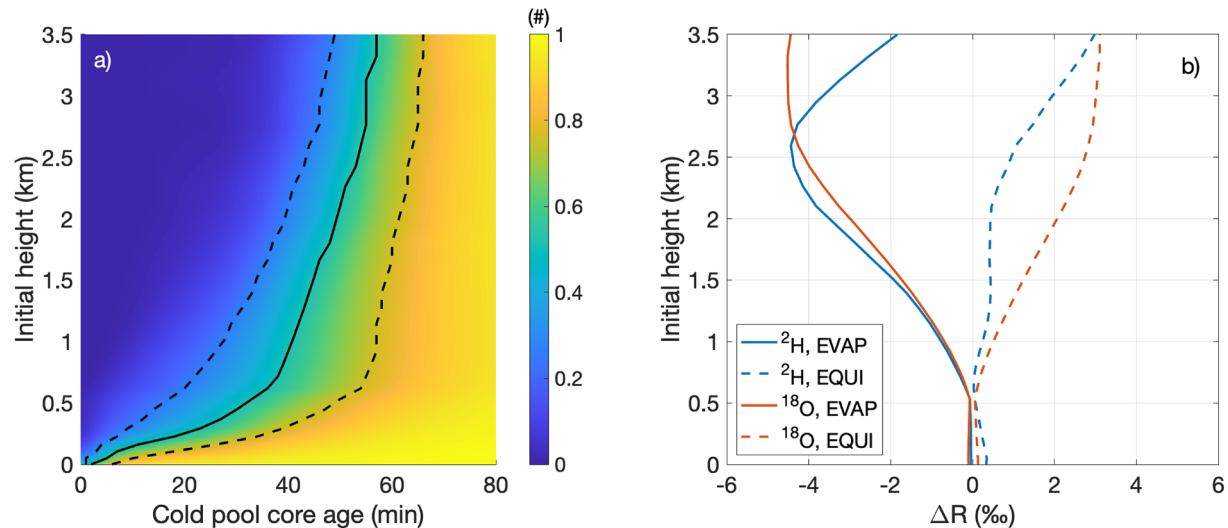

Figure 2. (a) Cumulative distribution function of ages of cold pool cores when downdraft particles enter them, shown as a function as the particles' initial heights (y-axis). The black line represents the median of the distribution, the dashed lines the 25th and 75th percentiles. (b) Total contribution of rain evaporation (continuous lines) and equilibration processes (dashed lines) to R_{2H} (blue) and R_{18O} (red).
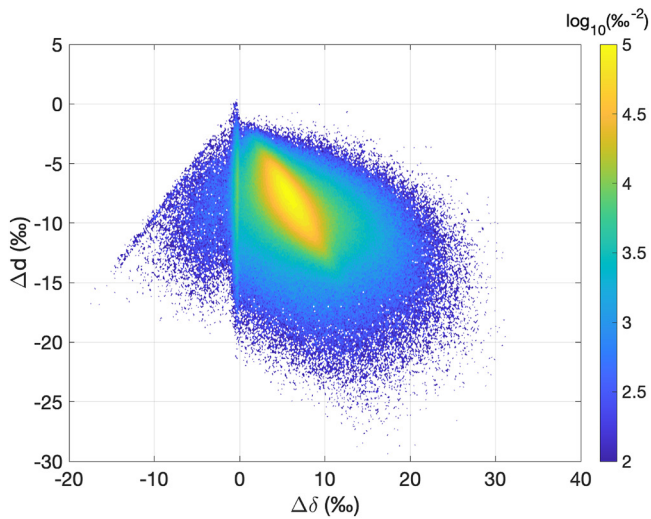
Figure 3. Base-10 logarithm of the bi-variate density function of differences between the near-surface values of water vapor δ^2H compared to the values in equilibrium with precipitation (x-axis) and differences between the near-surface values of water vapor deuterium excess and the hypothetical deuterium excess of vapor in equilibrium with precipitation (see text for more details).

The $\Delta\delta\Delta d$-diagram (see Section 2.6) for the control ensemble is then determined. For every grid box at the lowest model level where $r_p \geq 0.3$ g kg^{-1}, the same threshold used to identify cold pool cores, the isotopic composition of the rain and of the water vapor are saved. The former is divided by the equilibrium fractionation factor in order to compute the isotopic composition of the equilibrium vapor, $R_{p,eq} = R_{p,sfc}/\alpha_l$. Figure 3 represents the base-10 logarithm of the density function obtained by combining all the selected points across all the simulations of the control ensemble.

The vast majority of points are in the fourth quadrant, where ^2H of the water vapor is lower than the equilibrium value, but the deuterium excess is higher. According to the interpretation provided by Graf et al. (2019), this would suggest that the isotopic composition of the liquid-vapor system is strongly affected by kinetic fractionation due to rain evaporation.

Figures S1a and S1b in Supporting Information S1 suggest that the upper portion of the density function, the one closer to the first quadrant of the diagram, is mostly contributed to by raindrops with a smaller radius and lower precipitation rates compared to the lower portion. This is consistent with the interpretation that smaller droplets have a smaller equilibration time scale and would, therefore, be closer to equilibrium than larger droplets (Bolin, 1959; Lee & Fung, 2008).

Figures S1c–S1f in Supporting Information S1 also show that the area near the maximum of the density function is largely contributed to by small-radius raindrops generated by relatively shallow and young clouds, likely deepening cumulonimbus clouds in their developing stage.

A model II linear regression conducted over all the points in the $\Delta\delta\Delta d$-diagram suggests a slope $\Delta d/\Delta\delta = -0.73$, which is substantially lower than the values of -0.31 reported by Graf et al. (2019), and -0.30 determined by Graf (2017). These discrepancies can likely be attributed to the differences in the cases examined: tropical isolated convective storms in this study, and mid-latitude cold fronts in the other cases.

Finally, the sensitivity to changes in the CCN concentration is addressed. Following the same methods used to construct Figure 1, the properties of the particles from the experiments NC10 and NC1000 are examined. Figures 4a–4d are constructed in exactly the same way as Figures 1a and 1c, except that they refer to the experiment NC10 (NC1000). Similarly to Figure 1, points for which the density of particles is lower than $10^{-1.75}$ m^{-2} are ignored. Compared to the control case, the lower threshold used here is due to the fact that only one simulation per sensitivity experiment is considered instead of a 5-simulation ensemble.

The figures show that varying CCN concentrations affects the contributions of equilibration, particularly for R_{2H}. In this case, the height where the contributions become positive changes significantly compared to Figure 1a. Changes are also observed for the contribution to R_{18O}, although these are mostly in magnitude and not in sign.

4. Discussion

The role of different physical processes in modulating the isotopic composition of precipitation-driven downdrafts was examined in Torri (2021). However, the methods used in that work did not allow to differentiate between various microphysical processes, thus leaving some important questions unanswered. The results shown in Section 3 provide some insights on how equilibration and evaporation affect the water vapor isotopic composition of convective downdrafts.

Figures 1b and 1d represent the contributions of rain evaporation to the total derivative of $\ln R_{2H}$ and $\ln R_{18O}$, respectively. The plots suggest that evaporation tends to have a consistently depleting effect on downdraft
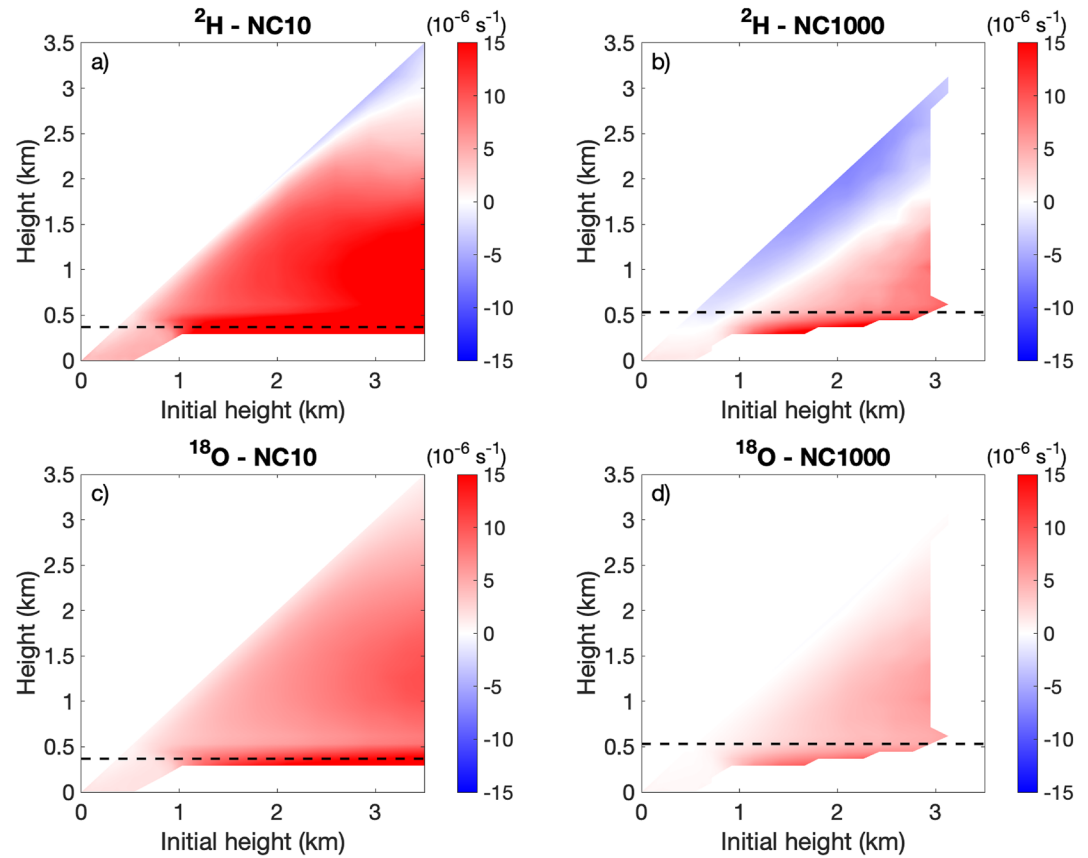
Figure 4. Same as Figures 1a and 1c, but for the sensitivity experiment (a and c) NC10 and (b and d) NC1000.

isotopes. This is intuitive since heavier isotopes tend to accumulate in the liquid phase (Stewart, 1975). In addition, from Equations 4 and 2, it is possible to show that:

$$\frac{S_{x,ev}}{r_x} - \frac{S_{v,ev}}{r_v} = \frac{S_{v,ev}}{r_v} \left[\left(\frac{f_x D_{x,v}}{f D_v} \right) \left(\frac{R_l}{\alpha_l R_v} \right) - 1 \right]. \tag{7}$$

Given that the heavier isotope diffusivities are smaller than those of the lighter isotope, Equation 7 suggests that evaporation has a depleting effect even when rain and vapor are in isotopic equilibrium.

The behavior of equilibration processes is a bit more complex to interpret. Figures 1a and 1c suggest that equilibration enriches water vapor in the first part of the downdraft. This would imply that $\delta^{18}O_v$ and, in particular, δ^2H_v are greater than the equilibrium value in the first part of the downdraft and lower in the second part. This is corroborated by directly comparing the isotopic composition of the vapor and the values of the vapor that would be in equilibrium with rain at different heights (Figure S2 in Supporting Information S1). Although their sampling method was different, something similar was also observed by Risi et al. (2020, see their Figure 4b).

In order to explain the reasons for this complex behavior, the age of the cold pool cores, and therefore of the rain shafts responsible for them, is examined in Figure 2a. The figure suggests that downdraft particles with initial heights greater than 1 km begin their descent when the parent cloud is in a mature stage. Considering that the terminal velocity of precipitation is greater than downdraft speeds (e.g., Kamburova & Ludlam, 1966; Knupp, 1988; Schiro & Neelin, 2018), it is likely that precipitation originates at greater altitudes from vapor that is much more depleted than the vapor below 3 km. When that precipitation comes in contact with downdraft vapor at lower altitudes, the vapor isotopic abundances are larger than the those that would be in equilibrium with rainfall. This might explain why equilibration tendencies are negative for the first half of the downdraft particles descent, particularly for ^2H isotopes.

As particles continue descending in the downdraft, rain evaporation enriches the isotopic composition of droplets. In addition, the equilibrium fractionation ratio decreases for increasing temperatures and, therefore, with decreasing height (Figure S3 in Supporting Information S1). This implies that the concentration of water vapor isotopes in downdrafts quickly becomes lower than that of the equilibrium vapor, which makes equilibration processes change sign and have an enriching effect.

One of the consequences of the alternating signs of equilibration tendencies can be appreciated in Figure 2b. A comparison between the dashed and the continuous lines suggests that, as far as microphysical processes in downdrafts are concerned, rain evaporation plays a greater role than equilibration in determining the final isotopic composition of a downdraft and, possibly, of rainfall. Following the interpretation of the $\Delta\delta\Delta d$-diagram given by Graf et al. (2019), this conclusion is further supported by Figure 3.

Finally, Figure 4 suggests that, while valid, the conclusions reached about the overall role of equilibration might be contextual to microphysical parameters, such as CCN concentration and the distribution of raindrop sizes. One factor that could explain this behavior is the difference in rain evaporation rates in the sensitivity experiments and the control ensemble (Figure S4 in Supporting Information S1). In the case of NC10, evaporation rates are significantly larger than in the control ensemble, potentially making it easier for raindrops to become much more enriched compared to the value required to be in equilibrium with vapor. The opposite is true for NC1000, although the difference in rain evaporation rates compared to the control ensemble appears more modest.

5. Conclusions

Water vapor isotopes are becoming an increasingly popular tool to study atmospheric convective systems. Although a considerable amount of data has been collected through the years, their interpretation is often made difficult by uncertainties surrounding the role that different physical processes play in modulating the isotopic composition of water vapor. This study aims at contributing to the effort of providing a process-based understanding of the behavior of water vapor isotopes in deep convective systems. The particular focus is on how microphysical processes, such as rain evaporation and equilibration, affect the isotopic composition of convective downdrafts.

Using a combination of cloud-resolving model simulations and Lagrangian diagnostics, it was shown that, for ^{2}H vapor isotopes, equilibration tends to have a depleting effect in the initial half of a downdraft life cycle and an enriching one in the second part. For ^{18}O, equilibration has mostly an enriching effect, although of a smaller magnitude compared to that for ^{2}H isotopes. For both isotopes, evaporation has a depleting effect which is consistent throughout the life cycle of a downdraft. Furthermore, it was shown that equilibration has an overall smaller effect compared to evaporation. Finally, the sensitivity of the results to CCN concentrations was tested, and it was shown that lower concentrations lead to greater enrichment of both water isotopes in vapor from equilibration processes.

Data Availability Statement

The data used in this paper are available at https://zenodo.org/record/6852224.

References

Aemisegger, F., Spiegel, J. K., Pfahl, S., Sodemann, H., Eugster, W., & Wernli, H. (2015). Isotope meteorology of cold front passages: A case study combining observations and modeling. *Geophysical Research Letters*, *42*(13), 5652–5660. https://doi.org/10.1002/2015gl063988

Arakawa, A. (2004). The cumulus parameterization problem: Past, present, and future. *Journal of Climate*, *17*(13), 2493–2525. https://doi.org/10.1175/1520-0442

Betts, A. K., & Silva Dias, M. F. (1979). Unsaturated downdraft thermodynamics in cumulonimbus. *Journal of the Atmospheric Sciences*, *36*(6), 1061–1071. https://doi.org/10.1175/1520-0469

Blossey, P. N., Kuang, Z., & Romps, D. M. (2010). Isotopic composition of water in the tropical tropopause layer in cloud-resolving simulations of an idealized tropical circulation. *Journal of Geophysical Research*, *115*(D24). https://doi.org/10.1029/2010jd014554

Bolin, B. (1959). On the use of tritium as a tracer for water in nature. Retrieved from https://www.osti.gov/biblio/4290366

Bolot, M., Legras, B., & Moyer, E. J. (2013). Modelling and interpreting the isotopic composition of water vapour in convective updrafts. *Atmospheric Chemistry and Physics*, *13*(16), 7903–7935. https://doi.org/10.5194/acp-13-7903-2013

Bony, S., Risi, C., & Vimeux, F. (2008). Influence of convective processes on the isotopic composition (δ^{18}O and δD) of precipitation and water vapor in the tropics: 1. Radiative-convective equilibrium and Tropical Ocean–Global Atmosphere–Coupled Ocean-Atmosphere response experiment (TOGA-COARE) simulations. *Journal of Geophysical Research*, *113*(D19), D19305. https://doi.org/10.1029/2008jd009942

Frank, W. M. (1983). The cumulus parameterization problem. *Monthly Weather Review*, *111*(9), 1859–1871. https://doi.org/10.1175/1520-0493(1983)111<1859:tcpp>2.0.co;2

Friedman, I., Machta, L., & Soller, R. (1962). Water-vapor exchange between a water droplet and its environment. *Journal of Geophysical Research*, *67*(7), 2761–2766. https://doi.org/10.1029/jz067i007p02761

Fujita, T. T. (1985). *The downburst: Microburst and macroburst. SMRP research paper 210*. University of Chicago.

Fujita, T. T. (1986). *DFW microburst on August 2, 1985. SMRP research paper 217*. University of Chicago.

Galewsky, J., Steen-Larsen, H. C., Field, R. D., Worden, J., Risi, C., & Schneider, M. (2016). Stable isotopes in atmospheric water vapor and applications to the hydrologic cycle. *Reviews of Geophysics*, *54*(4), 809–865. https://doi.org/10.1002/2015rg000512

Garstang, M., & Betts, A. K. (1974). A review of the tropical boundary layer and cumulus convection: Structure, parameterization, and modeling. *Bulletin of the American Meteorological Society*, *55*(10), 1195–1205. https://doi.org/10.1175/1520-0477(1974)055<1195:arottb>2.0.co;2

Gedzelman, S. D., & Arnold, R. (1994). Modeling the isotopic composition of precipitation. *Journal of Geophysical Research*, *99*(D5), 10455–10471. https://doi.org/10.1029/93jd03518

Graf, P. (2017). *The effect of below-cloud processes on short-term variations of stable water isotopes in surface precipitation* (Unpublished doctoral dissertation). ETH Zurich. https://doi.org/10.3929/ethz-b-000266387

Graf, P., Wernli, H., Pfahl, S., & Sodemann, H. (2019). A new interpretative framework for below-cloud effects on stable water isotopes in vapour and rain. *Atmospheric Chemistry and Physics*, *19*(2), 747–765. https://doi.org/10.5194/acp-19-747-2019

Hoefs, J. (2015). *Stable isotope geochemistry*. Springer.

Iacono, M. J., Delamere, J. S., Mlawer, E. J., Shephard, M. W., Clough, S. A., & Collins, W. D. (2008). Radiative forcing by long-lived greenhouse gases: Calculations with the AER radiative transfer models. *Journal of Geophysical Research*, *113*(D13), D13103. https://doi.org/10.1029/2008jd009944

Jeevanjee, N., & Romps, D. M. (2015). Effective buoyancy, inertial pressure, and the mechanical generation of boundary-layer mass flux by cold pools. *Journal of the Atmospheric Sciences*, *72*(8), 3199–3213. https://doi.org/10.1175/JAS-D-14-0349.1

Kamburova, P. L., & Ludlam, F. H. (1966). Rainfall evaporation in thunderstorm downdraughts. *Quarterly Journal of the Royal Meteorological Society*, *92*(394), 510–518. https://doi.org/10.1002/qj.49709239407

Khairoutdinov, M. F., & Randall, D. A. (2003). Cloud resolving modeling of the ARM Summer 1997 IOP: Model formulation, results, uncertainties, and sensitivities. *Journal of the Atmospheric Sciences*, *60*(4), 607–625. https://doi.org/10.1175/1520-0469(2003)060<0607:crmota>2.0.co;2

Knupp, K. R. (1988). Downdrafts within high plains cumulonimbi. Part II: Dynamics and thermodynamics. *Journal of the Atmospheric Sciences*, *45*(24), 3965–3982. https://doi.org/10.1175/1520-0469(1988)045<3965:dwhpcp>2.0.co;2

Lee, J.-E., & Fung, I. (2008). "Amount effect" of water isotopes and quantitative analysis of post-condensation processes. *Hydrological Processes*, *22*(1), 1–8. https://doi.org/10.1002/hyp.6637

Mlawer, E. J., Taubman, S. J., Brown, P. D., Iacono, M. J., & Clough, S. A. (1997). Radiative transfer for inhomogeneous atmospheres: RRTM, a validated correlated-k model for the longwave. *Journal of Geophysical Research*, *102*(D14), 16663–16682. https://doi.org/10.1029/97jd00237

Moore, M., Blossey, P. N., Muhlbauer, A., & Kuang, Z. (2016). Microphysical controls on the isotopic composition of wintertime orographic precipitation. *Journal of Geophysical Research: Atmospheres*, *121*(12), 7235–7253. https://doi.org/10.1002/2015jd023763

Nie, J., & Kuang, Z. (2012). Beyond bulk entrainment and detrainment rates: A new framework for diagnosing mixing in cumulus convection. *Geophysical Research Letters*, *39*(21). https://doi.org/10.1029/2012gl053992

Nusbaumer, J., Wong, T. E., Bardeen, C., & Noone, D. (2017). Evaluating hydrological processes in the Community Atmosphere Model Version 5 (CAM5) using stable isotope ratios of water. *Journal of Advances in Modeling Earth Systems*, *9*(2), 949–977. https://doi.org/10.1002/2016ms000839

Pfahl, S., Wernli, H., & Yoshimura, K. (2012). The isotopic composition of precipitation from a winter storm—A case study with the limited-area model COSMO$_{iso}$. *Atmospheric Chemistry and Physics*, *12*(3), 1629–1648. https://doi.org/10.5194/acp-12-1629-2012

Risi, C., Muller, C., & Blossey, P. (2020). What controls the water vapor isotopic composition near the surface of tropical oceans? Results from an analytical model constrained by large-eddy simulations. *Journal of Advances in Modeling Earth Systems*, *12*(8), e2020MS002106. https://doi.org/10.1029/2020ms002106

Risi, C., Muller, C., & Blossey, P. (2021). Rain evaporation, snow melt, and entrainment at the heart of water vapor isotopic variations in the tropical troposphere, according to large-eddy simulations and a two-column model. *Journal of Advances in Modeling Earth Systems*, *13*(4), e2020MS002381. https://doi.org/10.1029/2020ms002381

Salamalikis, V., Argiriou, A., & Dotsika, E. (2016). Isotopic modeling of the sub-cloud evaporation effect in precipitation. *Science of the Total Environment*, *544*, 1059–1072. https://doi.org/10.1016/j.scitotenv.2015.11.072

Schiro, K. A., & Neelin, J. D. (2018). Tropical continental downdraft characteristics: Mesoscale systems versus unorganized convection. *Atmospheric Chemistry and Physics*, *18*(3), 1997–2010. https://doi.org/10.5194/acp-18-1997-2018

Schlemmer, L., & Hohenegger, C. (2014). The formation of wider and deeper clouds as a result of cold-pool dynamics. *Journal of the Atmospheric Sciences*, *71*(8), 2842–2858. https://doi.org/10.1175/JAS-D-13-0170.1

Siebesma, P., Bony, S., Jakob, C., & Stevens, B. (Eds.) (2020). *Clouds and climate: Climate science's greatest challenge*. Cambridge University Press. https://doi.org/10.1017/9781107447738

Stewart, M. K. (1975). Stable isotope fractionation due to evaporation and isotopic exchange of falling waterdrops: Applications to atmospheric processes and evaporation of lakes. *Journal of Geophysical Research*, *80*(9), 1133–1146. https://doi.org/10.1029/jc080i009p01133

Thompson, G., Field, P. R., Rasmussen, R. M., & Hall, W. D. (2008). Explicit forecasts of winter precipitation using an improved bulk microphysics scheme. Part II: Implementation of a new snow parameterization. *Monthly Weather Review*, *136*(12), 5095–5115. https://doi.org/10.1175/2008mwr2387.1

Tompkins, A. M. (2001). Organization of tropical convection in low vertical wind shears: The role of water vapor. *Journal of the Atmospheric Sciences*, *58*(6), 529–545. https://doi.org/10.1175/1520-0469(2001)058<0529:ootcil>2.0.co;2

Tompkins, A. M., & Craig, G. C. (1998). Radiative–convective equilibrium in a three-dimensional cloud-ensemble model. *Quarterly Journal of the Royal Meteorological Society*, *124*(550), 2073–2097. https://doi.org/10.1256/smsqj.55012

Torri, G. (2021). On the isotopic composition of cold pools in radiative-convective equilibrium. *Journal of Geophysical Research: Atmospheres*, *126*(10), e2020JD033139. https://doi.org/10.1029/2020jd033139

Torri, G., & Kuang, Z. (2016a). A Lagrangian study of precipitation-driven downdrafts. *Journal of the Atmospheric Sciences*, *73*(2), 839–854. https://doi.org/10.1175/JAS-D-15-0222.1

Torri, G., & Kuang, Z. (2016b). Rain evaporation and moist patches in tropical boundary layers. *Geophysical Research Letters*, *43*(18), 9895–9902. https://doi.org/10.1002/2016gl070893

Torri, G., Kuang, Z., & Tian, Y. (2015). Mechanisms for convection triggering by cold pools. *Geophysical Research Letters*, *42*(6), 1943–1950. https://doi.org/10.1002/2015gl063227

Tremoy, G., Vimeux, F., Soumana, S., Souley, I., Risi, C., Favreau, G., & Oï, M. (2014). Clustering mesoscale convective systems with laser-based water vapor δ^{18}O monitoring in Niamey (Niger). *Journal of Geophysical Research: Atmospheres*, *119*(9), 5079–5103. https://doi.org/10.1002/2013jd020968

Wakimoto, R. M., Kessinger, C. J., & Kingsmill, D. E. (1994). Kinematic, thermodynamic, and visual structure of low-reflectivity microbursts. *Monthly Weather Review*, *122*(1), 72–92. https://doi.org/10.1175/1520-0493

Wang, S., Zhang, M., Che, Y., Zhu, X., & Liu, X. (2016). Influence of below-cloud evaporation on deuterium excess in precipitation of arid central Asia and its meteorological controls. *Journal of Hydrometeorology*, *17*(7), 1973–1984. https://doi.org/10.1175/jhm-d-15-0203.1

Yamaguchi, T., Randall, D. A., & Khairoutdinov, M. F. (2011). Cloud modeling tests of the ultimate–macho scalar advection scheme. *Monthly Weather Review*, *139*(10), 3248–3264. https://doi.org/10.1175/mwr-d-10-05044.1

Zhu, G., Zhang, Z., Guo, H., Zhang, Y., Yong, L., Wan, Q., et al. (2021). Below-cloud evaporation of precipitation isotopes over mountains, oases, and deserts in arid areas. *Journal of Hydrometeorology*, *22*(10), 2533–2545. https://doi.org/10.1175/jhm-d-20-0170.1